ELSEVIER

Journal of Nuclear Materials 273 (1999) 164–170

journal of nuclear materials

www.elsevier.nl/locate/jnucmat

Native vacancy migrations in zircon

R.E. Williford [a,*], W.J. Weber [a], R. Devanathan [a], A.N. Cormack [b]

[a] *Materials Department, Pacific Northwest National Laboratory, M.S. K2-444, P.O. Box 999, Richland, WA 99352, USA*
[b] *New York State College of Ceramics, Alfred University, Alfred, NY 14802, USA*

Received 25 August 1998; accepted 20 January 1999

Abstract

Energy minimization methods were used to simulate the migration of Zr, Si, and O vacancies in zircon ($ZrSiO_4$). Two sets of interatomic potentials were employed for comparison: one with O–Si–O three-body terms for the SiO_4, and one without. Results for Si were inconclusive, but consistent with maintaining the integrity of the SiO_4 molecular units. Both Zr and O vacancies can migrate on three-dimensional sublattice networks, thus supporting the experimentally observed diffusional isotropy. The predicted Zr vacancy migration energy (1.16–1.38 eV) was in good agreement with experiment if supplemented by Zr vacancy formation via Schottky or Frenkel defects (6.21–12.28 eV/defect). Oxygen vacancy migration energies were predicted to be 0.99–1.16 eV, somewhat lower than the experimental value of 4.64 eV measured in natural zircons, which thus may include significant contributions from vacancy formation mechanisms at 3.31–6.52 eV/defect.

PACS: 61.80.–X; 61.80.AZ; 61.82.MS

1. Introduction

Zircon ($ZrSiO_4$) is a familiar material in the waste isolation community. It forms as one of several crystalline phases in glass ceramic waste forms [1–5], has been observed as a corrosion product on HLW glass [6], and is a prominent actinide-bearing phase in the crystallized core melt of Chernobyl [7,8]. Zircon has also been proposed as a ceramic host material for the immobilization and disposal of excess weapons-grade Pu in US [9,10] and high-actinide wastes in Russia [7,11]. The soundness of this recommendation is based on the fact that natural zircon is extremely durable. Individual grains undergo many cycles of environmental erosion, weathering, and physical contact, but exhibit only limited dissolution or abrasion. Zircons are the oldest terrestrial materials to have been dated: 4.1 to 4.3 billion years [12–14]. Its suitability as a host phase is further supported by its ability to incorporate large amounts (10% or greater) of Pu [15–18] and U [11]. The extensive substitution of Pu for Zr was demonstrated by the synthesis of isostructural $PuSiO_4$ [19].

Although recent experimental [20–23] and computational [24,25] work has addressed the diffusivity and heats of solution for various actinides (Pu, U, Th) in zircon, none of those investigations have treated the fundamental question of native vacancy migration paths and energetics. It is important to determine these activation energies so that comparisons between theory and experiment are possible. Such comparisons enable the understanding of the basic diffusion mechanisms that are responsible for transport in zircon, and can be critical for designing or tailoring waste isolation hosts to minimize the release of actinides to the environment.

Computer simulation of the fundamental native vacancy migration processes is the main objective of this paper. In the balance of the paper, we first briefly outline the crystal structure of zircon. This is followed by a description of the computational tools employed to simulate zirconium, silicon, and oxygen vacancy migrations in zircon. Migration paths and energies are then described and quantified using several empirical potentials in the GULP code [26]. Discussion of these new results includes comparisons with the available data, and is followed by the conclusions.

* Corresponding author. Tel.: +1-509 375 2956; fax: +1-509 375 2186; e-mail: re_williford@pnl.gov.

0022-3115/99/$ – see front matter
PII: S0022-3115(99)00026-4

2. Zircon crystal structure

The crystal structure of zircon has been previously described in detail [27,28], and will only be briefly reviewed here. The unit cell is tetragonal, with $a = b = 0.661$ nm and $c = 0.598$ nm. The space group is $I4_1/amd$, and there are 24 atoms in the complete unit cell. The prominent structural units are chains of alternating edge-sharing SiO_4 tetrahedra and ZrO_8 triangular dodecahedra extending along the c axis, as shown in Fig. 1. Octahedral voids are present that contain no cations. The Zr is eight-coordinated with oxygen, with four bonds of 0.215 nm and four of 0.229 nm. Si–O bonds are 0.162 nm. Within the SiO_4 tetrahedra, the shortest O–O edges (0.243 nm) are shared with the dodecahedra, but the 0.275 nm O–O edges are unshared. Within the ZrO_8 dodecahedra, the 0.249 nm O–O edges shown in Fig. 1 are shared with other dodecahedra, but the 0.307 and 0.284 nm O–O edges are unshared. It will be shown below that the latter are the most important for oxygen vacancy migration. Clinographic views of zircon are shown in Fig. 2.

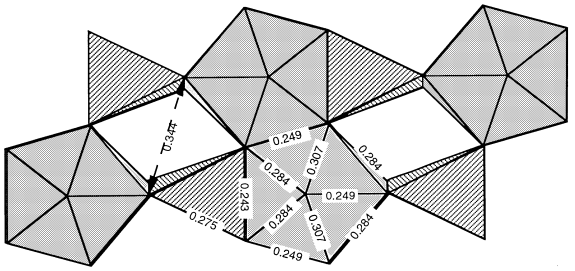

Fig. 1. Polyhedral representation of zircon structure, showing SiO_4 tetrahedra (ruled) and ZrO_8 dodecahedra (shaded). Numbers show O–O distances in nm, with oxygen located at each polyhedron corner. Zr and Si atoms not shown for clarity. The c axis is horizontal on the page.

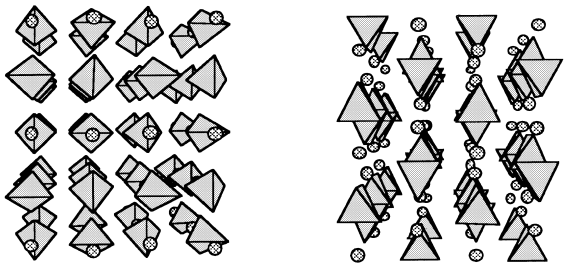

Fig. 2. Clinographic views of zircon with the c axis (left) and a axis (right) extending out of the page. SiO_4 tetrahedra are shaded, Zr atoms are cross-hatched.

3. Computational methods

The GULP code (General Utility Lattice Program) [26,29] was used in this investigation to simulate the energetics and structures of perfect lattices and of defects. GULP is an energy minimization code based on the Born model, where energy is partitioned into long ranged Coulombic interactions computed via Ewald summation techniques, and short ranged atomic pair and three-body potentials. The code is unique in that it optimizes the use of crystal symmetry to make structure generation easier and to speed up calculations.

Isolated defects in extended solids were addressed using the Mott–Littleton approximation [30]. In this well-known method, the crystal surrounding the defect is divided into three concentric spherical regions of progressively larger radii. Region 1 contains the defect per se, where interactions are treated explicitely at the atomic level, and ions are relaxed in response to the defect. In Region 2a, the ions are assumed to reside in a harmonic well and respond accordingly to the defect forces. This approximation is only valid for small perturbations in Region 2a (i.e., Region 1 must be of sufficiently large radius) and requires that the bulk lattice be relaxed prior to introduction of the defect (a standard procedure). Individual ion displacements are still treated in Region 2a, whereas only the implicit polarization of sublattices is considered in Region 2b. The defect energy is calculated as the energy difference between the defected (E_{def}) and perfect (E_{perf}) lattices, and corrected for the energy of interstitials or vacancies at infinite separation from the lattice: $E_{defect} = E_{def} - E_{perf} + E_{inf}$. Details of the computational method are given elsewhere, e.g., Ref. [31].

Charged defects polarize other ions in the lattice. Ionic polarization was modeled with the well-known Dick–Overhauser shell model [32]. This model treats the deformation polarization caused by distortion of the electron density in response to the charged defect, resulting in the development of a dipole moment. The model also includes the important coupling between short range repulsion and ion polarization, which prevents excessive polarization of the ion. A simple harmonic spring model was used to represent the separation of the electron cloud from the ionic core. Within an ion, the core-shell charge partitioning determines electronic polarizability. The net ionic (core + shell) charge may depart from formal charges in order to approximate the effects of partial covalency.

An important GULP capability for the present work was the ability to perform transition state searches, where an energetic 'saddle point' is found by seeking atomic positions with a specified number of negative eigenvalues in Hessian [26]. Thus, calculations of the activation energies for vacancy migrations could be routinely performed in two steps. In the first step, the

defect energy of a single vacancy was calculated as described above, using standard energy minimization techniques. In the second step, an interstitial was placed between the two vacancies which were the initial and final positions of the migrating ion corresponding to the migrating vacancy, and a transition state with one negative eigenvalue was sought. The difference between the defect energies of these two calculations gave the activation energy for vacancy migration. The results of such calculations are described below.

4. Interatomic potentials for zircon

For comparative purposes, three sets of potentials were considered: (1) Gay and Rohl (G&R) [33], (2) Chandley, Clark, Angel and Price (CCAP) [34], and He and Cormack (H&C) [25]. Each set is described below. Unless otherwise stated, all potentials were of the Buckingham form, with cutoff radii of 1.0 nm.

The Gay and Rohl (G&R) [33] potentials were designed for investigating equilibrium crystal facets during crystal growth of zircon. The oxygen ions were modeled with a harmonic spring shell model, while rigid ions were used for the Zr and Si. G&R treated the SiO_4 tetrahedra as molecular units and used a Morse potential for the Si–O interactions, with a 0.2 nm cutoff for this fairly strong bond. A three-body O–Si–O bond bending term was used to help maintain structural integrity at surfaces, with a Si–O cutoff of 0.2 nm and an O–O cutoff of 0.3 nm. This three-body O–O cutoff was increased to 0.35 nm in the present work. G&R modeled other O–O interactions using a Buckingham potential they developed especially for zircon, with a C-parameter appearing small enough to prevent redundancy with the three-body terms. Although the three-body terms in the G&R potentials can lead to serious computational instabilities in some cases, we have continued to use them (a) because of our previous success with the reduced coordination systems associated with radiation induced ion displacements [35], (b) because the free surfaces encountered during crystal growth can be viewed as the 'largest defects' with the lowest coordination, and (c) because vacancy migrations also require reduced coordination.

The Chandley, Clark, Angel and Price (CCAP) [34] potentials also included an O–Si–O three-body term, but did not treat the silica tetrahedra as molecular units. Their Si–O Buckingham potential was previously developed for silicates [36], and also contained a relatively small C-parameter. Their O–O potential was the well established potential derived by Catlow using quantum techniques [37]. As in the G&R potentials, only the oxygen ion was treated with a harmonic spring core-shell model.

The H&C potentials were also based on previous work [36–39], and were used in He and Cormack's study of disorder in zircon [25]. The H&C potentials were similar to the CCAP potentials, except that they did not include an explicit three-body term. The same O–O [37] and Si–O [36] Buckingham potentials were used, along with a Zr–O potential from [38].

Table 1
Results for three sets of potentials[a]

Potential	G&R	H&C	Data
Lattice energy	−263.30	−237.83	–
Volume (prim.)	0.1318	0.1304	0.1304
Cell size (a,b)	0.668	0.631	0.661
Cell size (c)	0.591	0.642	0.598
c_{11}	43.83	45.01	42.3
c_{33}	52.69	50.98	49.0
c_{44}	11.09	11.28	11.3
c_{12}	6.60	6.28	7.3
c_{13}	14.05	17.77	14.9
V_{Zr}^{4-}	79.32	83.36	–
V_{Si}^{4-}	105.18	105.74	–
$V_{O}^{\bullet\bullet}$	27.33	21.05	–
O_i''	−14.28	−14.43	–

[a]Cell size is in nm, volume of the primitive cell is in nm^3, energies are in eV, and elastic constants are in units of 10^{10} Pa. Data are from Refs. [27,40].

Some basic features of GULP output for these three potential sets are shown in Table 1. The G&R and H&C potentials are in generally good agreement with each other and with the experimental data. Exceptions are the lattice energy and the oxygen vacancy energy, $V_O^{\bullet\bullet}$, for the G&R potentials, due to the strong Si–O bonds in their Morse potentials. It was not possible to reproduce the CCAP results [34] for vacancy formation energies (85.41, 105.81, and 24.31 eV for Zr, Si, and O, respectively), and the predicted cell anisotropy was incorrect. Furthermore, the presence of three-body terms introduced code convergence problems when Si vacancies were simulated, as in the G&R potentials (see below). Because the CCAP potential set also contained features of both other sets, it was therefore not considered further.

5. Vacancy migration energies

All defect calculations were performed using lattices that had been previously equilibrated at constant pressure and 0 K (Table 1). The Region 1 radius was taken as 0.92 nm, or about 300 ion cores. Results for Zr, Si, and O vacancy migration energies are shown in Table 2, where the O jump distances correspond with Fig. 1. In general, the G&R potentials gave slightly larger oxygen vacancy migration energies than the H&C potentials, apparently due in part to the three-body and Si–O terms discussed above. Conversely, the H&C cation vacancy migration energies were slightly larger than those for the G&R potentials.

Table 2
Results for native vacancy migration energies (eV) in zircon[a]

Ion	Dist. (nm)	Description	G&R	H&C
Zr	0.365	In plane of Fig. 3	1.16	1.38
Zr	0.557	Into page in Fig. 3	8.84	10.24
Si	0.365	In plane of Fig. 3	–	0.43*
Si	0.557	Into page in Fig. 3	–	9.42
O	0.307	Unshared ZrO_8	19.51	4.80
O	0.249	Shared ZrO_8–ZrO_8	17.72	2.77
O	0.243	Shared ZrO_8–SiO_4	1.28	0.90
O	0.344	SiO_4 to SiO_4	1.27	1.74
O	0.275	Unshared SiO_4	1.39	0.86
O	0.284	Unshared ZrO_8	1.16	0.99

[a]Distances and descriptions correspond to those in Figs. 1 and 3. G&R and H&C are the potential sets described above. 'Shared' and 'unshared' refer to polyhedra edges. The * entry is not a true saddle point (see text).

Only the two shortest cation jump distances are shown for Zr and Si, the shorter of the two being in the plane of Fig. 3 and the longer normal to that plane. Fig. 3 is a view along the ⟨1 1 1⟩ direction of a $2 \times 2 \times 2$ supercell to more clearly show these cation vacancy migration paths. Results for Zr are reasonably consistent between the potential sets. At first glance, calculations for the longer Zr migration path (0.557 nm) appear to be in good agreement with the data of Cherniak Hanchar and Watson's [21,22] for rare earth (Yb^{3+}, Dy^{3+}, Sm^{3+}) and tetravalent (U^{4+}, Th^{4+}, Hf^{4+}) ion diffusion in zircon. Their experimentally determined activation energies ranged between 7.5 and 8.7 eV over the temperature range of 1150–1650°C, compared to 8.84–10.24 eV calculated herein at 0 K. The vacancy migration energy of 8.4 eV obtained experimentally for Hf [21] is noteworthy because Hf has the same atomic radius and valence as Zr, and is easily substituted.

However, the shorter (0.365 nm) Zr migration path is more likely because of its much lower energy requirement (1.16–1.38 eV). Since the experimental methods (see below) indicate dominance by intrinsic defect formation, the difference in energies (e.g., $8.7 - 1.3 = 7.4$ eV) would be accounted for by Zr vacancy formation. Although He and Cormack's [26] calculation of Zr Frenkel formation energy (12.28 eV/defect) is slightly high, it is within the scatter between potential sets in Table 2. Zr vacancies can also be created by Schottky defect formation, computed at 6.21 eV/defect by He and Cormack [26]. Their results thus bracket the ~7.4 eV energy defecit noted above. Consequently, the shorter path should dominate Zr vacancy migration.

Cherniak et al. [21,22] also reported diffusional isotropy for the impurity cations studied, although this was actually inferred rather than measured for Hf. Diffusional isotropy would seem reasonable for Zr when the networks of atomic jumps for vacancy migrations are plotted, as in Fig. 4. Both cases form three-dimensional networks. Deviations of the saddle point positions from the centers of straight migration paths were small considering the lengths of the paths.

Results for Si vacancy migration were inconclusive. The code did not converge for the G&R potentials, apparently due to sustained oscillations in the local force fields as Si atoms were moved about while searching for the transition state. This probably occurred because of the short cutoff distances used in the molecular Si–O and

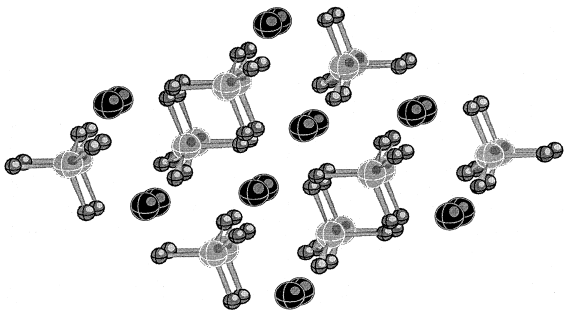

Fig. 3. View of zircon near the ⟨1 1 1⟩ axis. Large black spheres (Zr), large shaded spheres (Si), small shaded spheres (O). Atom sizes are distorted for clarity in viewing the cations in this $2 \times 2 \times 2$ supercell.

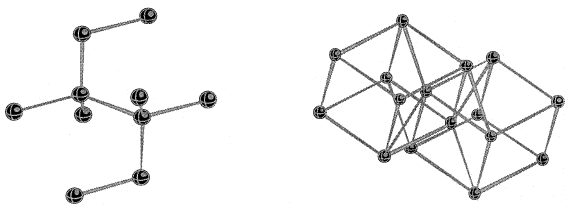

Fig. 4. Diagram of Zr vacancy migration paths, viewed near the c axis of $2 \times 2 \times 2$ supercells for clarity. Left = 0.365 nm (1.15–1.38 eV) shorter jumps, right = 0.557 nm (8.84–10.24 eV) longer jumps. Both networks are three dimensional and indicate diffusional isotropy of Zr.

three-body potentials for the SiO_4 tetrahedra, which essentially created a cusp as other potentials became more dominant beyond the cutoffs. Such discontinuities will defeat any Newton–Raphson minimizer routine. Results for the shortest vacancy migration path using the H&C potentials (Table 2) were again very low. The saddle points found in this case were slightly smaller than the Si vacancy energy, and may have represented low-lying vibrational modes. The result reported in Table 2 (i.e., 0.43*) is not a true saddle point, but rather the energy of a fixed Si interstitial at the center of the migration path between two Si vacancies, with the surrounding lattice relaxed. On the other hand, the 9.42 eV obtained for the longer (0.557 nm) path may be reasonable in light of observations that intact silica tetrahedra are detected via Raman spectroscopy even in fully amorphized zircon, indicating that a high activation energy is required to disrupt the tetrahedra for Si vacancy migration.

A total of six vacancy migration paths were investigated for oxygen. The jump distances in Table 2 correspond to those in Fig. 1. In the 0.344 nm case, the O vacancy moves nearly vertically across the void in Fig. 1, from one SiO_4 tetrahedron to another. The first two oxygen cases (0.307 and 0.249 nm) had very high activation energies because the O atom must jump between rows of Zr atoms, and thus do not appear energetically favorable. The differences in results are again expected to be caused by the effects of the Morse potential and three-body terms in the G&R potentials. The remaining cases had much smaller activation energies: 1.39–1.16 eV for the G&R potentials and 1.74–0.90 eV for the H&C potentials. From Fig. 1, it is easy to see that the shared SiO_4–ZrO_8 edges (0.243 nm) cannot form a complete diffusional network. The 0.344 and 0.275 nm cases (between SiO_4 tetrahedra and along unshared tetrahedra edges, respectively), had similar O vacancy migration energies. When taken together, these migration paths form a complete three-dimensional network (Fig. 5) with activation energy limited by the largest value (1.39 eV according to the G&R potentials, 1.74 eV by the H&C potentials).

Most interesting, however, is the network of oxygen vacancy migrations along the unshared ZrO_8 dodecahedra edges (Figs. 6 and 7), which requires an even lower activation energy of only 1.16 eV by the G&R potentials (0.99 eV by the H&C potentials). This is also a three-dimensional network, and is thus also consistent with experimental observations that oxygen diffusion in zircon is isotropic [23]. However, both sets of potentials predicted activation energies significantly lower than the experimental data: 4.64 eV [23]. This apparent discrepancy is addressed as follows. Watson and Cherniak [23] found that about 20% of their samples exhibited anomolously long 'diffusion tails', which they attributed in part to preexisting oxygen vacancies needed for charge

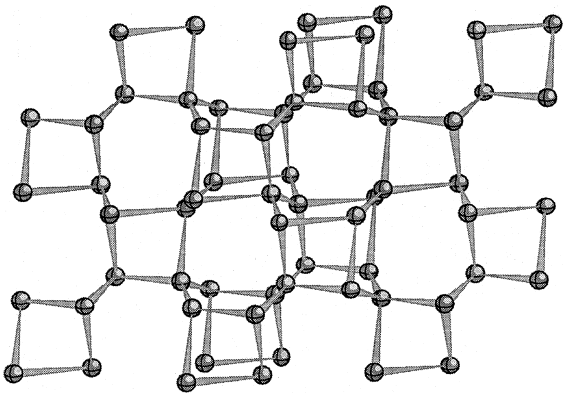

Fig. 5. Three-dimensional network of oxygen vacancy migration paths limited to the SiO_4 tetrahedra, composed of 0.344 nm jumps between tetrahedra and 0.275 nm jumps along unshared tetrahedra edges. Viewed near the c axis of a $2 \times 2 \times 2$ supercell, rotated 45° clockwise for clarity.

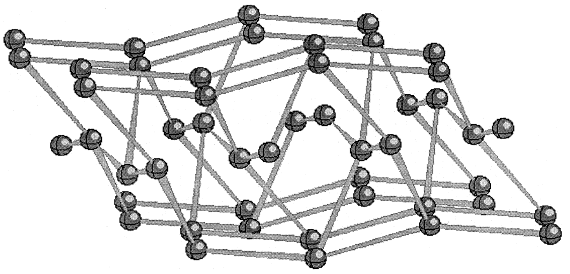

Fig. 6. Three-dimensional network of the oxygen migration paths along the unshared, 0.284 nm ZrO_8 dodecahedra edges of a $2 \times 2 \times 2$ supercell, with a lower activation energy of 0.99–1.16 eV. Viewed near the a axis for clarity.

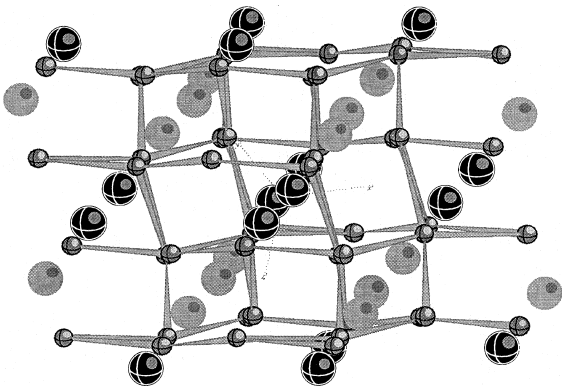

Fig. 7. Same as Fig. 6, but viewed near the c axis, and with Zr (large black spheres) and Si (large shaded spheres) shown for perspective.

balance with impurities in the optically clear, gem quality natural zircons they tested. They took great care to eliminate samples with preexisting vacancies from their data base. In their data analyses, they also discarded the long diffusional tails with lower Arrhenius slopes (smaller activation energies). It might thus be inferred that their samples could have been 'vacancy deficient', so that their results would contain a significant contribution from the *formation* of the oxygen vacancies that are needed to enable vacancy *migration* in the zircon. This inference is supported by the following arguments.

He and Cormack [25] computed the formation energies for a full range of intrinsic defects, and found that they were energetically favored in the following order: anion Frenkels, interstitials, Schottky, and cation Frenkels. Anion Frenkels thus provide the easiest means to create the necessary oxygen vacancies. Anion Frenkel formation requires 6.52 eV per defect by the G&R potentials and 3.31 eV per defect by the H&C potentials. These results nicely span the experimental data (4.64 eV), indicating that the latter could be dominated by vacancy *formation* energetics. If so, the lower vacancy *migration* energies reported in herein would be consistent with the available data.

6. Discussion and conclusions

GULP has many useful capabilities for modeling defects. The transition state search was a feature important for this work, since it yields saddle points for vacancy migrations. However, note that these saddle points depend on the empirical potentials employed. Although results seemed consistent, and subsequent checks (performed by relaxing an interstitial placed at the saddle point) confirmed the saddle point positions, it is always possible that other saddle points were not found. This was particularly true for the Si vacancy migrations. It would be advantageous for future work to include development of methods to locate all likely saddle points, even for very curved migration paths. Another useful development would be to find ways to eliminate the three-body terms, with the expectation of improving the results for Si. Also useful would be the development of minimization methodologies to more directly relate these empirical simulations to changes in electronic states as ions and vacancies migrate, thus enabling the eventual development of methods for fitting potentials to defects using, e.g., spectroscopic data. Note that the approach employed was essentially an extrapolation from the perfect lattice to the defect state, as are all similar approaches.

Both Zr and O vacancies can migrate on fully connected three-dimensional networks within the zircon lattice, thus supporting experimental observations of diffusional isotropy. Two distinct vacancy migration networks were identified for Zr, and two for O. Although both sets of potentials appeared to underpredict the available experimental data, results were reasonable when defect formation energies were also included, as indicated by the experimental methods. The predicted Zr vacancy migration energy for the shorter, lower energy (1.16–1.38 eV) path could be activated by Zr vacancy formation at 6.21–12.28 eV/defect for Schottky or Frenkel defects, respectively, which gives good agreement with the experimental data (7.5–8.7 eV). The oxygen vacancy migration energy was predicted to be as low as 0.99–1.16 eV, which is noticeably lower than the experimentally observed value of 4.64 eV. The low activation energies predicted herein would be a significant result if it could be proven that the zircon samples were initially free of oxygen vacancies, so that the experimental data were dominated by vacancy formation (3.31–6.52 eV/defect) rather than by vacancy migration energetics. It is clear that further improvements are desirable in the potentials and possibly in the data base itself.

Acknowledgements

This work was supported by the Environmental Management Science Program, Office of Environmental Management, US Department of Energy under Contract DE-AC06-76RLO 1830. The Pacific Northwest National Laboratory is operated by Battelle Memorial Institute for the US Department of Energy. We also wish to thank a reviewer for several suggestions that improved this paper.

References

[1] A.B. Harker, J.F. Flintoff, J. Am. Ceram. Soc. 68 (1985) 159.
[2] A.B. Harker, J.F. Flintoff, J. Am. Ceram. Soc. 73 (1990) 1901.
[3] X. Fen, J.E. Surma, C.G. Whitworth, R.C. Eschbach, G.L. Leatherman, Glass as a Waste Form and Vitrification Technology, Summary of an International Workshop, National Academy Press, Washington, 1996, p. 68.
[4] D.A. Knecht, T.P. O'Holleran, K. Vinjamuri, S.V. Raman, B.A. Staples, in Glass as a Waste Form and Vitrification Technology, Summary of an International Workshop, National Academy Press, Washington, 1996, p. 78.
[5] S.V. Raman, R. Bopp, T.A. Batcheller, Q. Yan, in: W.M. Murphy, D.A. Knecht (Eds.), Scientific Basis for Nuclear Waste Management XIX, Mater. Res. Soc. Symp. Proc. 412. Materials Research Society, Pittsbutgh, PA, 1996, p. 113.
[6] A. Abdelouas, J.L. Crovisier, W. Lutze, B. Grambow, J.C. Dran, R. Muller, J. Nucl. Mater. 240 (1997) 100.

[7] B.E. Burakov, E.B. Anderson, B.Ya. Galkin, V.A. Starchenko, V.G. Vasiliev, in: E. Merz, C.E. Walter (Eds.), Disposal of Weapons Plutonium, Kluwer Academic, The Netherlands, 1996, p. 85.
[8] B.E. Burakov, SafeWaste '93, vol. 2, 1993, p. 19.
[9] R.C. Ewing, W. Lutze, W.J. Weber, J. Mater. Res. 10 (1995) 243.
[10] R.C. Ewing, W. Lutze, W.J. Weber, in: E. Merz, C.E. Walter (Eds.), Disposal of Weapons Plutonium, Kluwer Academic, The Netherlands, 1996, p. 65.
[11] E.B. Anderson, B.E. Burakov, E.M. Paxhukin, Radoichim. Acta 60 (1993) 149.
[12] D.O. Froude, T.R. Ireland, P.D. Kinney, I.S. Williams, W. Compston, I.R. Williams, J.S. Meyers, Nature 304 (1983) 616.
[13] S. Moorbath, Nature 321 (1986) 725.
[14] R. Maas, P.D. Kinney, I.S. Williams, D.O. Froude, W. Compton, Geochim. Cosmochim. Acta 56 (1992) 1281.
[15] W.J. Weber, G.D. Maupin, Nucl. Instrum. Meth. B 32 (1988) 512.
[16] W.J. Weber, J. Mater. Res. 5 (1990) 2687.
[17] W.J. Weber, J. Am. Ceram. Soc. 76 (1993) 1729.
[18] W.J. Weber, R.C. Ewing, L.M. Wang, J. Mater. Res. 9 (1994) 688.
[19] C. Keller, Nukleonic 5 (1963) 41.
[20] D.J. Cherniak, W.A. Lanford, F.J. Ryerson, Geochim. Cosmochim Acta 55 (1991) 1663.
[21] D.J. Cherniak, J.M. Hanchar, E.B. Watson, Contrib. Minerol. Petrol. 127 (1997) 383.
[22] D.J. Cherniak, J.M. Hanchar, E.B. Watson, Chem. Geol. 134 (1997) 289.
[23] E.B. Watson, D.J. Cherniak, Earth Plan. Sci. Lett. 148 (1997) 527.
[24] C. Meis, J.D. Gale, Mater. Sci. Eng. B 857 (1998) 52.
[25] Y. He, A.N. Cormack, J. Nucl. Mater, submitted.
[26] J.D. Gale, J. Chem. Soc. Faraday Trans. 93 (1997) 629.
[27] A. Beltrin, S. Bohm, A. Flores-Riveros, J.A. Ingualada, G. Monros, J. Andres, J. Phys. Chem. 97 (1993) 2555.
[28] K. Robinson, G.V. Gibbs, P.H. Ribbe, Am. Mineral. 56 (1971) 782.
[29] J.D. Gale, Philos. Mag. B 73 (1996) 3.
[30] N.F. Mott, M.J. Littleton, Trans. Faraday Soc. 34 (1938) 485.
[31] W. Hayes, A.M. Stoneham, Defects and Defect Processes in Nonmetallic Solids, Wiley, New York, 1985.
[32] B.G. Dick, A.W. Overhauser, Phys. Rev. 112 (1958) 90.
[33] D.H. Gay, A.L. Rohl, J. Chem. Soc. Faraday Trans. 91 (1995) 925.
[34] P. Chandley, R.J.H. Clark, R.J. Angel, G.D. Price, J. Chem. Soc. Dalton Trans (1992) 1579.
[35] R.E. Williford, R. Devanathan, W.J. Weber, Nucl. Instrum. Meth. B 141 (1998) 94.
[36] M.J. Sanders, M. Leslie, C.R.A. Catlow, J. Chem. Soc. Chem. Commun. (1984) 1273.
[37] C.R.A. Catlow, Proc. Roy. Soc. A 333 (1977) 533.
[38] A. Dwivedi, A.N. Cormack, J. Solid State Chem. 79 (1989) 218.
[39] S.C. Parker, C.R.A. Catlow, A.N. Cormack, Acta. Crystallogr. B 40 (1984) 200.
[40] H. Ozkan, J. Appl. Phys. 47 (1976) 4772.